

Zoledronic acid modulates osteoclast apoptosis through activation of the NF- κ B signaling pathway in ovariectomized rats

Yu-Ting Cheng^{1,*} , Jian Liao^{1,*} , Qian Zhou¹, Hua Huo¹, Lucas Zellmer², Zheng-Long Tang¹, Hong Ma¹, Wei Hong³ and Dezhong Joshua Liao⁴

¹School/Hospital of Stomatology, Guizhou Medical University, Guizhou 550004, P.R. China; ²Masonic Cancer Center, University of Minnesota, Minneapolis, MN 55455, USA; ³Key Laboratory of Endemic and Ethnic Diseases, Guizhou Medical University, Ministry of Education, Guizhou 550004, P.R. China; ⁴Department of Pathology, Guizhou Medical University School of Medicine, Guizhou 550004, P.R. China

Corresponding authors: Jian Liao. Email: liaojian@gmc.edu.cn; Lucas Zellmer. Email: lzellmer@umn.edu

*These authors contributed equally to this work.

Impact statement

Osteoporosis is a prominent risk factor affecting the success of dental implant surgery. In recent years, ZOL has been introduced into the field of stomatology as a highly effective bone resorption inhibitor; ZOL effectively promotes the process of implant osseointegration. However, the specific regulatory mechanism of this drug on osteoclasts is still controversial and few studies have reported the mechanism of ZOL using *in vivo* animal experiments. The results of this study suggest that ZOL improves mandibular bone growth in rats. Moreover, our results indicate that ZOL modulates osteoclast apoptosis through activation of the nuclear factor kappa-B signalling pathway in ovariectomized rats. The purpose of this study is threefold: to understand the regulatory mechanism of ZOL in inhibiting bone resorption at the molecular level, to provide a theoretical basis for its local clinical application, and to promote the utilization of ZOL in the field of dental implants.

Abstract

Bone mass loss (osteoporosis) seen in postmenopausal women is an adverse factor for implant denture. Using an ovariectomized rat model, we studied the mechanism of estrogen-deficiency-caused bone loss and the therapeutic effect of Zoledronic acid. We observed that ovariectomized-caused resorption of bone tissue in the mandible was evident at four weeks and had not fully recovered by 12 weeks post-ovariectomized compared with the sham-operated controls. Further evaluation with a TUNEL assay showed ovariectomized enhanced apoptosis of osteoblasts but inhibited apoptosis of osteoclasts in the mandible. Zoledronic acid given subcutaneously as a single low dose was shown to counteract both of these ovariectomized effects. Immunohistochemical staining showed that ovariectomized induced the protein levels of RANKL and the 65-kD subunit of the NF- κ B complex mainly in osteoclasts, as confirmed by staining for TRAP, a marker for osteoclasts, whereas zoledronic acid inhibited these inductions. Western blotting showed that the levels of RANKL, p65, as well as the phosphorylated form of p65, and I κ B- α were all higher in the ovariectomized group than in the sham and ovariectomized + zoledronic acid groups at both the 4th- and 12th-week time points in the mandible. These data collectively suggest that ovariectomized causes bone mass loss by enhancing apoptosis of osteoblasts and inhibiting apoptosis of osteoclasts. In osteoclasts, these cellular effects may be achieved by

activating RANKL-NF- κ B signalling. Moreover, zoledronic acid elicits its therapeutic effects in the mandible by counteracting these cellular and molecular consequences of ovariectomized.

Keywords: Zoledronic acid, osteoporosis, osteoclast, osteoblast, NF- κ B signaling pathway, RANKL

Experimental Biology and Medicine 2021; 246: 1727–1739. DOI: 10.1177/15353702211011052

Introduction

In recent years, implant denture has been a primary tactic to restore missing teeth as it causes little harm to natural teeth, allows a good recovery of mastication and, compared with other approaches, is more feasible and less uncomfortable.^{1,2} However, this tactic requires tooth extraction,

whereas certain bone diseases that affect bone metabolism, such as osteoporosis, can cause destruction of alveolar bones and thus affect the healing of alveolar fossae after tooth extraction.^{3,4} While osteoporosis is a general adversarial factor for bone implant surgery,^{5,6} postmenopausal osteoporosis (PMOP) has been a main focus of medical

research in recent years as it has become increasingly problematic due to the rising elderly population worldwide, which poses a major public health problem itself.⁷⁻⁹ In rats, ovariectomy (OVX) affects bone wound healing, especially in the early phase (roughly the first four weeks), although healing can still occur eventually.^{10,11}

In PMOP, estrogen deficiency increases the level of the receptor activator nuclear κ B ligand (RANKL) secreted by osteoblasts in the bone.¹² RANKL binds in a competitive manner to RANK on the surface of osteoclasts to activate the tumor necrosis factor receptor-associated factors (TRAFs), including TRAF6. Through a signalling cascade, TRAF6 activates the transcription factor NF- κ B pathway, which in turn activates genes regulating the differentiation of osteoclasts.¹³⁻¹⁵ As a result, formation and activation of osteoclasts are enhanced, thus enhancing bone resorption and resulting in the loss of bone mass,¹⁶ as illustrated in Figure 1.

Bisphosphonates have been widely used in clinics to treat metastatic bone cancer, Paget disease, and osteoporosis.^{17,18} A conventional dose is about 100 μ g/kg, but the optimal doses and durations still await further optimization¹⁹ for different pathologies since long-term treatment with a high dose has been shown to cause bisphosphonate-related osteonecrosis of jaw, especially in the mandible.²⁰ Zoledronic acid (ZOL), a third-generation nitrogen-containing bisphosphonate, has been shown to be the most effective bisphosphonate in the treatment of osteoporosis.²¹ ZOL has also been shown to effectively promote bone formation around implanted teeth,^{22,23} inhibit bone resorption, and potentially promote bone formation mainly through its impact on osteoclasts and osteoblasts.²⁴ For these reasons, ZOL has gradually been introduced into stomatology as a highly effective bone resorption inhibitor.^{22,23} Mechanistically, the two nitrogen atoms in the

imidazole side chain of ZOL have a high affinity to hydroxyapatite in bone and can directly interfere with the adhesion of osteoclasts to the bone's surface, causing ultra-structural changes of osteoclasts that eventually lead the cells to apoptosis.^{25,26} However, detailed molecular mechanisms underlying these cellular effects of ZOL remain to be elucidated as relevant reports are not consistent.^{27,28} Furuya *et al.* have observed that osteoblasts can directly contact osteoclasts, promoting the transformation of R-type osteoclasts with bone resorption into the N-type osteoclasts without bone resorption.²⁹ Greiner *et al.* have shown that when primary osteoblasts are co-cultured with osteoclast-like cells, the two cell types interact with each other; ZOL added into the culture facilitates this interaction and has better effects on both cell types as well, compared with its efficacy in the culture of each cell type.³⁰ As a result, ZOL, especially at a high dose, promotes not only apoptosis of osteoclasts but also differentiation of osteoblasts that subsequently benefits implanted teeth.³⁰ However, these effects do not seem to involve NF- κ B signaling.³⁰ In addition, animal studies have also shown that a single systemic administration of ZOL can increase the bone mineral density around dental implants.³¹⁻³³

In a previous study, we observed that ZOL can inhibit the differentiation and function of osteoclasts *in vitro*. These effects are associated, in a dose- and time-dependent manner, with an inhibition of expression of the NF- κ B, JNK, and some genes regulating osteoclast formation, including the calcitonin receptor (calcitonin receptor, CTR), RANK, and activated T nuclear factor (nuclear factor of activated T cells, NFATc1).³⁴ In the present study, we further determined whether these cellular and molecular effects of ZOL observed *in vitro* would also occur in animals that receive a single low dose of ZOL.

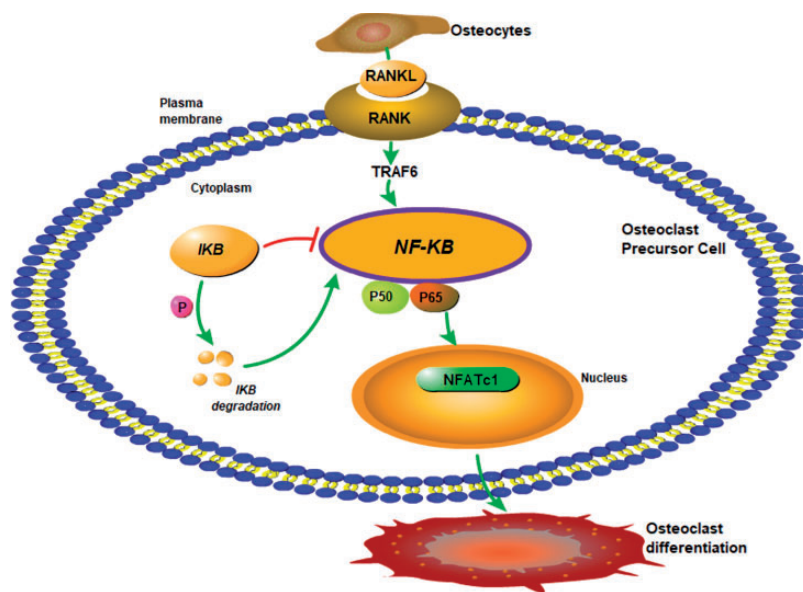


Figure 1. Involvement of RANK-NF- κ B signalling in the differentiation of osteoclasts in osteoporosis. RANKL secreted by mature osteoblasts binds to and activates RANK on osteoclast precursors, activating TRAF6 that in turn activates the NF- κ B signalling pathway. As a downstream event, NFATc1 is activated and enters into the nucleus to regulate expression of genes related to osteoclast differentiation and maturation. (A color version of this figure is available in the online journal.)

Materials and methods

Reagents and instruments

Reagents were acquired as follows: ZOL was purchased from Novartis Pharma Stein AG, Switzerland (ST303). ELISA kits (PINP: E-EL-R1414c, CTX-I: E-EL-1456c) were obtained from Elabscience Biotechnology Co., Ltd, Wuhan, China, whereas a TUNEL apoptosis kit (KGA702-A) was purchased from KeyGEN BioTECH Co., Ltd, Jiangsu, China. A hematoxylin and eosin (H-E) staining solution (G1121), a Masson trichrome staining solution (G1340), a TRAP staining kit (G1492), a BCA protein concentration determination kit, and a polyacrylamide gel cast system were purchased from Solarbio Science Technology Co., Ltd, Beijing, China. Polyvinylidene difluoride (PVDF) membranes were obtained from EMD Millipore. Primary antibodies against NF- κ B p65 (bsm-33117M) and RANKL/CD254 (bs-0747R), used for both immunohistochemical (IHC) staining and Western blotting (WB), were purchased from Biosynthesis Biotechnology Co., Ltd, Beijing, China. Secondary antibodies and associated kits for IHC were from Zhongshan Jinqiao Biotechnology Co., Ltd, Beijing, China. Primary antibodies against p65 (#8242), phospho-p65 (p-p65, #3033), I κ B α (#4812), and phospho-I κ B α (p-I κ B α at Ser 32, #2859) used for WB were purchased from Cell Signaling Technology, USA. β -actin antibody (bs-0061R) used for WB was purchased from Biosynthesis Biotechnology Co., Ltd, Beijing, China. A secondary antibody for WB (#014-091S) was obtained from PMK Bioprimary Co., Ltd, Wuhan, China, whereas a chemiluminescence solution used for WB was obtained from ECL, Millipore, USA. A stripping buffer (#SW3020) was purchased from Technology Co., Ltd, Beijing, China. A dental X-ray machine was purchased from SIRONA, Germany. A fluorescence and light microscope from Nikon ECLIPSE CI, Japan, was used for capturing IHC images. A chemiluminescence imaging system from SYNGENE Co., Ltd GeneGnome XRQ NPC, England, was used for capturing protein signals from WB membranes, whereas an enzyme-labeling instrument from Bio-Tek ELX800, USA, was used for determination of optical density (OD) of the signals from WB membranes.

Animals

Seventy-two adult female SD rats of specific pathogen free (SPF) grade weighing 250–300 g supplied by our university's animal facility were housed in polypropylene cages (four animals per cage) in the facility under standard conditions (22–25°C and light on from 7 a.m. to 7 p.m.), with food and water supplied ad libitum. The animals were randomly and equally (24/group) divided into the sham-operated group, the OVX group, and the OVX plus ZOL group, referred to as "the ZOL group" for simplicity. After one week of acclimation, OVX was performed under anesthesia in sterile conditions as described before.³⁵ Three months after OVX, all rats were anesthetized with an intraperitoneal injection of 3% sodium pentobarbital at a dose of 35 mg/kg in sterile conditions, followed by extraction and saturation of the left mandibular molars with local

compression applied to stop the bleeding. Buprenorphine (Temgesic) was administered during the recovery from surgery for pain relief. The ZOL group immediately received a single subcutaneous injection of ZOL at a dose of 20 μ g/kg, while the other two groups received saline as the control. The rats were then placed in a heat-controlled environment for recovery and fed with a soft diet for the remaining duration of the experiment. Bodyweights were regularly measured, which showed changes of less than 10%. No adverse events were observed, such as uncontrolled pain or inflammation.

The animal study was approved by the Animal Experimental Ethics Committee of Guizhou Medical University (no.1603096) with the animal use under an approved protocol (SCXK; 2015-0001) to Jian Liao. All experimental procedures were performed in accordance with the guidelines of the International Council on Research Animal Care as well as the "Guide for the Care and Use of Laboratory Animals" by the National Institute of Health of the United States.

Blood sample collection and processing

Under anesthesia as described above, 5 mL of blood were collected from the abdominal aorta of each rat from half of the animals in each group at four weeks, and from the other half of the animals at 12 weeks, after the tooth extraction. Collection of such a large amount of blood was more convenient from the aorta than from other body sites.³⁶ The sampling was conducted around 8 a.m. to avoid influence by the circadian rhythm. After the blood was immediately spun at 10,000 \times g for 10 min at room temperature, serum was collected and transferred into a new tube and stored immediately at –80°C until its use. The animals were then euthanized using CO₂ asphyxiation.

Dental X-ray imaging

A dental X-ray machine was used to take dental images at conditions of 70-kV voltage and 7-mA current for an irradiation time of 0.03 s.

Bone tissue preparation for H-E staining and Masson staining

The mandible tissue around the site of tooth extraction was collected from the animal with the soft tissue carefully separated using a saline-saturated gauze. A portion of the bone tissue was placed at –80°C for Western blot analyses. The remaining tissue was fixed for 48 h with a 4% paraformaldehyde solution and, after X-ray imaging analysis, was decalcified for approximately seven weeks until a syringe needle could easily penetrate the bone. The decalcified specimens underwent a routine paraffin embedding procedure carried out by the pathology department of our hospital. Paraffin sections of about 4–5 μ m in thickness were prepared for H-E staining, Masson trichrome staining, and IHC staining. For Masson trichrome staining to visualize collagen fibres, which is routinely conducted in our pathology department, paraffin sections were dewaxed with xylene and rehydrated with deescalating concentrations

of ethanol and then with water, followed by staining with Weigert's solution and then fuchsin staining of cytoplasm/muscle/erythrocyte.

IHC staining and positivity quantification

After deparaffinization with xylene, removal of xylene, and rehydration with decreasing concentrations of ethanol and then with water, the tissue sections were treated with a 0.25% trypsin solution for 30 min for antigen retrieval and then with 3% H₂O₂ in deionized water to exhaust the endogenous peroxidase. After blocking with a normal goat serum for 30 min, the sections were incubated with a primary antibody at a dilution of 1:50 overnight at 4°C. The next morning, the sections were prewarmed at 37°C for 30 min and then incubated with the corresponding secondary antibody that had been pre-conjugated with a streptavidin-biotin complex (SABC). A diaminobenzidine solution was applied onto the sections for color development, followed by a light hematoxylin counterstaining to visualize the nuclei. Three quick washes with phosphate-buffered saline (PBS) were applied between each step. The sections were then rehydrated with increasing concentrations of ethanol, submerged in xylene, and then mounted with a neutral gum. Under a light microscope, the total OD of the positive staining in an area was measured using the Image ProPlus 6.0 image analysis software; five randomly selected areas were measured for each section from each animal for statistical comparisons.

TUNEL staining for detection of apoptotic cells and TRAP staining for osteoclasts

Paraffin sections were dewaxed and rehydrated as described above, followed by treatment with a protein kinase K to digest nuclear proteins so that chromosomal DNA was well exposed. After exposure with a 3% H₂O₂ solution for 30 min to exhaust the endogenous peroxidase, the sections were incubated with a reaction solution of deoxyribonucleotide terminal transferase to append a peroxidase-conjugated nucleotide at the 3-OH end of cleaved DNA in apoptotic cells. After three quick washes, a diaminobenzidine solution was applied to the section for color development, followed by a light hematoxylin counterstaining of the nuclei. The sections were then rehydrated and mounted with a neutral gum as described above. The positive TUNEL staining was imaged and quantified as described for the IHC staining. The TRAP staining kit was then used to stain TRAP, an osteoclast marker, according to the manufacturer's instructions. The cells determined as positive for TRAP staining contained characteristic red, granular material. TRAP-positive multinucleated cells with >3 nuclei identified under a positive microscope were considered osteoclasts.

ELISA analyses of serum biomarkers for bone turnover

Each standard sample or serum sample (100 µL, diluted 50 times) was added to a well of a 96-well plate, followed by incubation at 37°C for 90 min. The samples were then removed from the wells and 100 µL of a working solution

of biotinylated antibody was added in, followed by incubation at 37°C for 60 min. After three quick washes with PBS, 100 µL of an enzyme-conjugate working solution was added and incubated at 37°C for 30 min. After the wells were washed five times with PBS, 90 µL of a substrate solution was added, followed by incubation at 37°C for 15 min. After the addition of 50 µL of termination solution, the OD at 450 nm wavelength was measured using an instrument for the enzyme-labeling. The OD values of the serial standard samples were used to plot a standard curve with which the concentration of the biomarker in each serum sample was calculated.

Protein preparation and WB

Each frozen bone tissue (50–100 mg) was put into a ceramic grinding bowl and poured into liquid nitrogen to make the bone fragile; a ceramic grinding rod was then used to finely grind the bone. The fine bone tissue was then put into an Eppendorf tube with addition of 200 µL of a RIPA lysate buffer containing a cocktail of protease inhibitors, followed by iterations of pipetting the tissue on ice. After centrifuging the tube at 12,000 r/min for 10 min at 4°C, the supernatant was collected as the protein sample, followed by determination of the protein concentration using a BCA kit. A 12% of polyacrylamide gel containing sodium dodecyl sulfate (SDS) was made; 30 µg of each protein sample was loaded into a well, with a pre-stained protein marker loaded into the first well. After electrophoresis of the gel in the presence of SDS (SDS-PAGE), the fractionated proteins were electro-transferred onto a PVDF membrane. The membrane was incubated with 5% skim milk in PBS at room temperature for 1.5 h and then a primary antibody was applied, followed by overnight incubation at 4°C. While all primary antibodies were diluted at 1:800, the β-actin antibody used to control the protein loading was diluted to 1:2000. After three washes with PBS again, a sheep anti-rabbit secondary antibody or a sheep anti-mouse secondary antibody, diluted to 1:15000, was applied at room temperature for 2 h, followed by applying an enhanced chemiluminescence solution (ECL) onto the membrane to develop a fluorescent signal. Three washes with PBS were applied between each step. The fluorescence was captured using a Gene Gnome Imaging System, followed by quantification of the fluorescent intensity using an ImageJ analysis software. When the WB was performed to detect a phosphorylated form of p65 or IκB-α, the antibody complex was removed from the membrane with a stripping buffer and then reused for a second round of WB for detecting the corresponding total protein. All experiments were carried out three times to obtain a mean and standard deviation (SD).

Statistical analyses

All quantitative data were presented as the mean ± SD. With the GraphPad Prism 6.0 statistical software, one-way ANOVA or two-way ANOVA were used to compare each group and the Tukey's post-test was carried out for multiple comparisons. A *P*-value less than 0.05 was set as the cut-off for statistical significance.

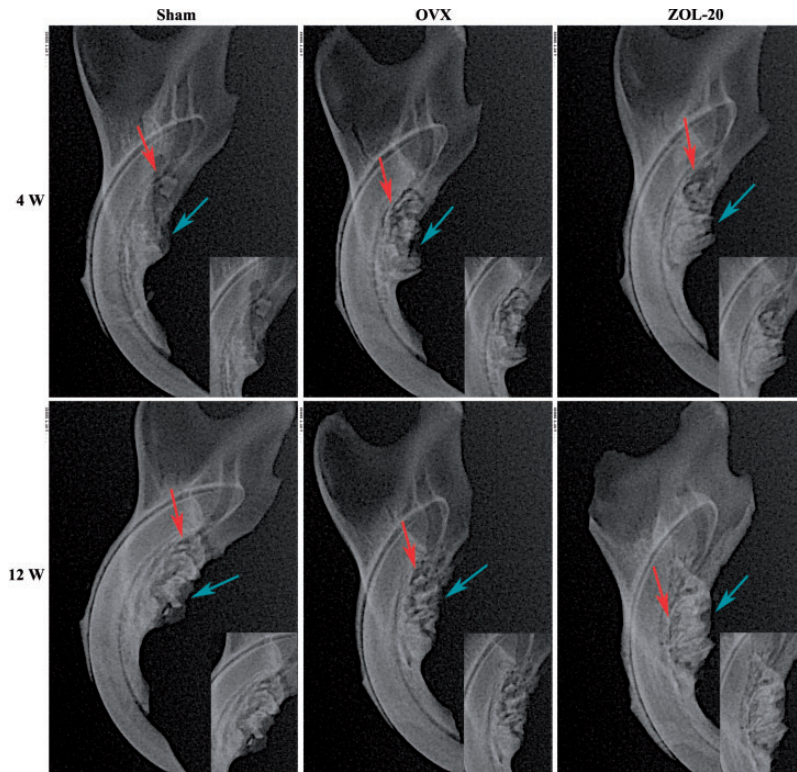


Figure 2. X-ray imaging of rat mandibles in the Sham, OVX, and ZOL groups at 4 and 12 weeks after tooth extraction. Note that the bone mineral density (red arrows) at the bottom of the alveolar fossa was higher in the ZOL group, was higher than in the OVX group, especially at 12 weeks, but was similar between the ZOL and Sham groups. On the other hand, alveolar ridge absorption (blue arrows) was obvious in the OVX group, especially at the fourth week, but was less evident in the sham group and not obvious in the ZOL group. The bone healing of the two groups was already complete at 12 weeks. (A color version of this figure is available in the online journal.)

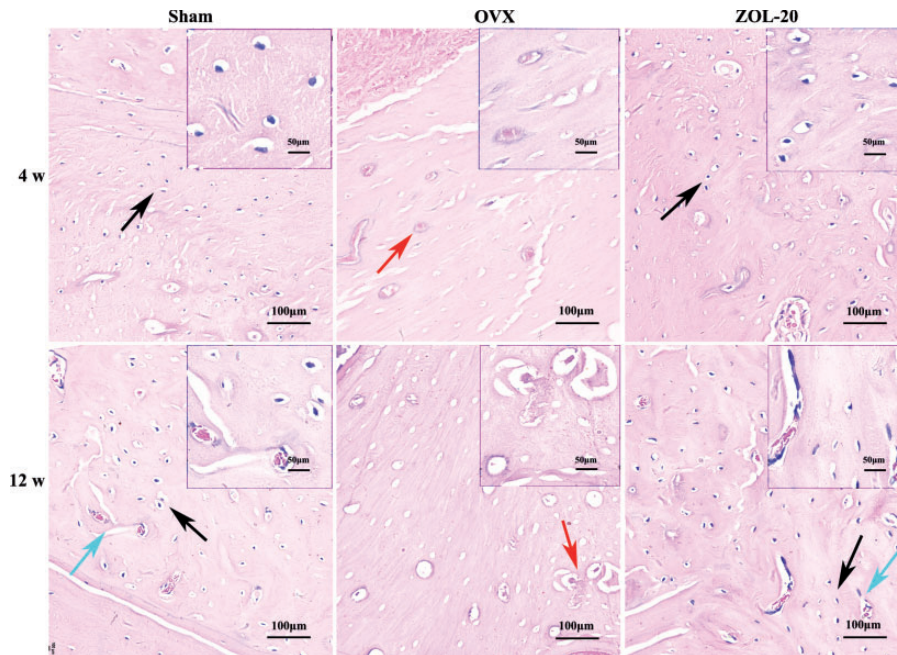


Figure 3. Histology of the mandible. Although the bone in each group is still more loose and less dense at the 4th week than the 12th week time point, a larger number of bone resorption lacunae and osteoclasts (red arrow) are discerned in the OVX group than in the sham and ZOL groups, and more osteocytes (black arrow) are found in the sham and ZOL groups. Neovascularization (blue arrow) can be discerned 12 weeks post OVX, especially in the sham and ZOL group. (A color version of this figure is available in the online journal.)

Results

Changes in X-ray imaging of the alveolar fossa in the mandible

X-ray images showed that the alveolar bone density in the mandible was pronouncedly decreased with a fuzzy trabecular appearance in the OVX group at four and 12 weeks post OVX, compared with the corresponding counterparts in the sham and ZOL groups (Figure 2). Especially at the 12th week, the ZOL group showed a higher mineral density than the sham group, while the degree of alveolar bone absorption was decreased among the two groups. Although the alveolar bone resorption was discerned in all three groups at the fourth week, the resorption was much milder in the sham and ZOL groups at the later time point compared with the OVX group (Figure 2). On the other hand, new bone formation found at the bottom of

the extraction pit was more evident in the ZOL group, especially at the later time point. These observations together indicate that 12 weeks post OVX, the bone wound healing is almost complete in the sham and ZOL groups while it is much slower in the OVX group (Figure 2).

Histopathological changes of the mandible

H-E staining revealed that the bone of each group was more loose and less dense at the fourth week than the later time point, as expected (Figure 3). Immature braided bone and rich collagen fibres, featured by its blue hematoxylin staining (Figure 4), were less abundant in the Sham and ZOL groups than in the OVX group, which could be discerned at four weeks and more so at 12 weeks post OVX. In contrast, the mature bone, featured by its red eosin staining (Figure 4), showed the opposite. The bone trabecular structure was thinner and often broken in the OVX group but

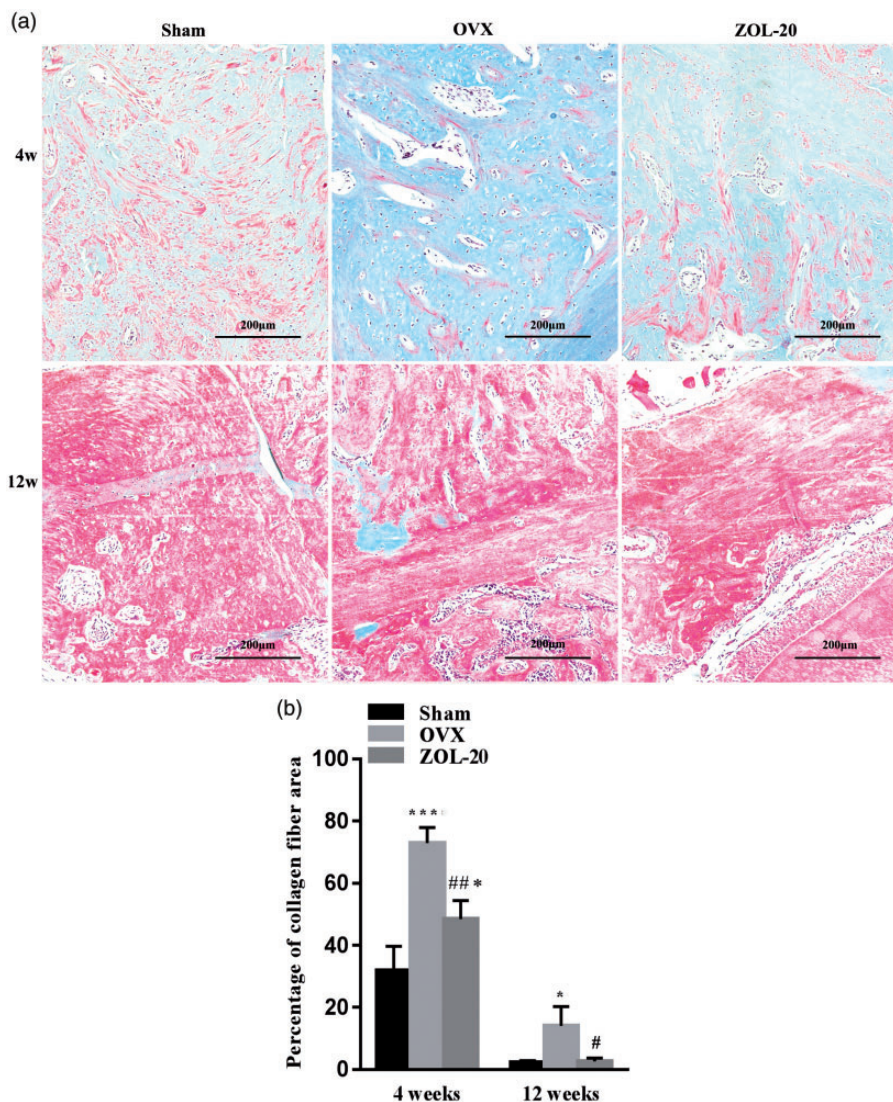


Figure 4. Masson staining of collagen fibres in the mandible, in which mature bone appears red, whereas immature braided bone that is fraught with collagen fibres appears blue (a). Quantification of stained collagen (b) shows that at the fourth-week time point, the OVX group has an abundance of collagen when compared with the sham group, whereas ZOL decreases the abundance of collagen; the collagen abundance was still more than the sham group. The collagen abundance shows little difference among the three groups 12 weeks post OVX. (Data are presented as mean \pm SD. * and *** indicate a $P < 0.05$ and < 0.001 , respectively, when compared with the Sham group; # and ## indicate a $P < 0.05$ and 0.01 , respectively, when compared with OVX group.) (A color version of this figure is available in the online journal.)

was normal in the sham and ZOL groups, especially at the fourth week (Figure 3). Moreover, the OVX group showed more osteoclasts that were distinctive by their polynuclei, much larger cellular size, and locations in the bone matrix compared to the sham and ZOL groups that showed more osteocytes embedded deeply in the bone tissue and were smaller in size with only one nucleus. These morphological features collectively suggest that OVX causes bone mass loss by increasing the number of osteoclasts and decreasing the number of osteoblasts, especially at the earlier time point. ZOL counteracts these OVX-causing effects to help the healing of the OVX-caused bone damage and even enhances the bone growth when compared with the sham-operated rats.

Effect of OVX and ZOL on apoptosis of osteoblasts and osteoclasts

TUNEL staining identified more apoptotic osteoblasts but less apoptotic osteoclasts in the OVX group than in the sham group, especially at the fourth-week time point (Figures 5 and 6). As aforementioned, these two cell types were located at different areas of the bone with osteoclasts stained for TRAP, which confirmed that those TUNEL-positive cells that were very large and had multiple nuclei were indeed osteoclasts (Figure 6(b)). These data indicate that OVX causes bone-mass loss by both increasing bone resorption and decreasing bone growth, as expected, especially during the early period after OVX. At the fourth week, the number of osteoblasts in the ZOL group was

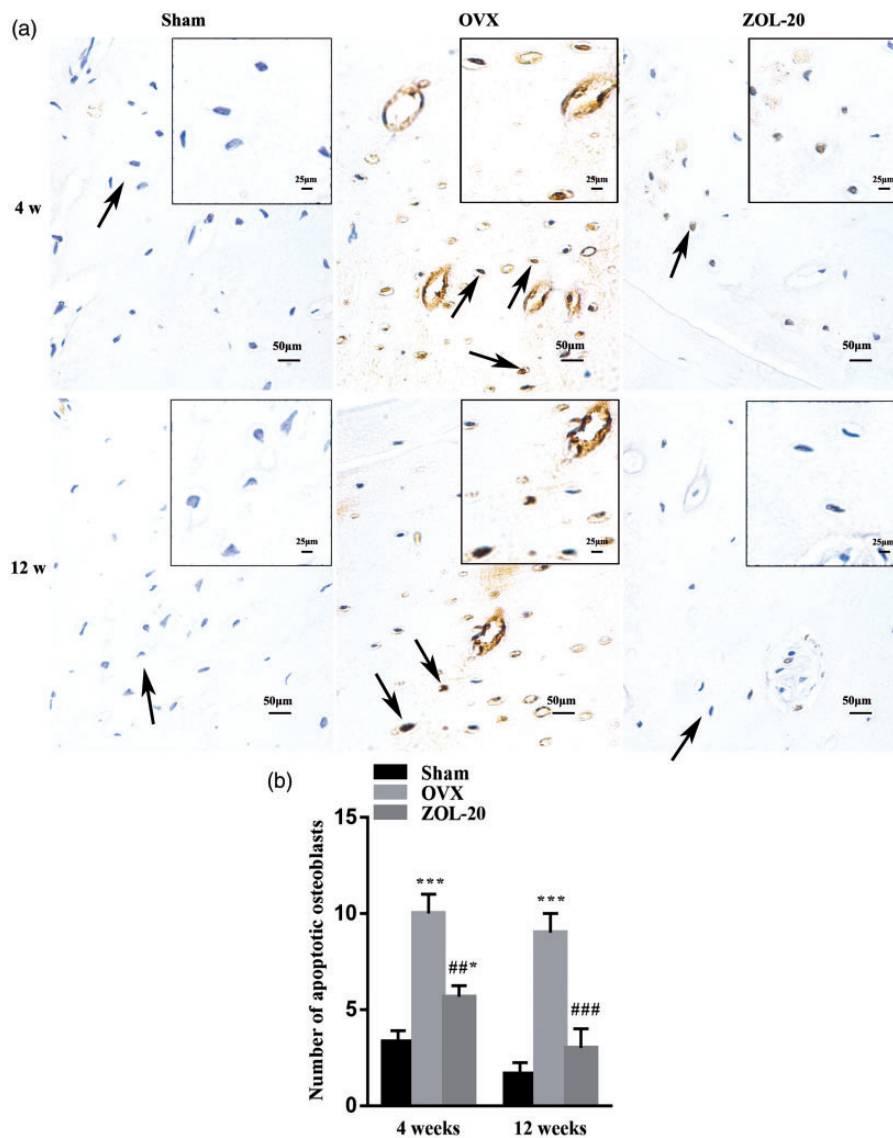


Figure 5. TUNEL staining detecting apoptotic osteoblasts in the osteoblast-abundant areas of the mandible. Note that the number of apoptotic osteoblasts (arrows) is more abundant in the OVX group than in the sham and ZOL groups, especially at the fourth-week time point (a), with the average staining intensity of five randomly selected areas per animal quantified and statistically compared (b). (Data are presented as mean \pm SD. * and *** indicate a $P < 0.05$ and 0.001 , respectively, when compared with the Sham group; ## and ### indicate a $P < 0.01$ and 0.001 , respectively, when compared the OVX group with the ZOL group.). (A color version of this figure is available in the online journal.)

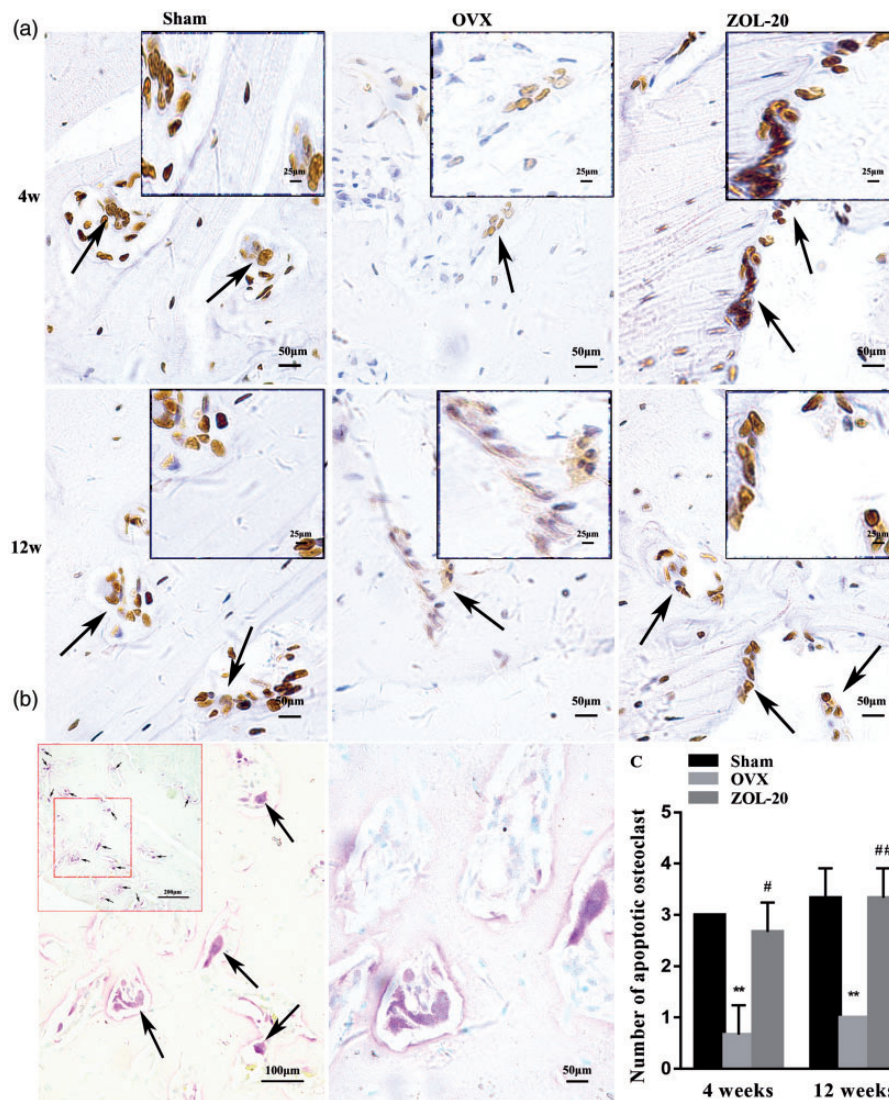


Figure 6. Detection of apoptotic osteoclasts with a TUNEL assay and with TRAP staining in the mandible. Note that the number of apoptotic osteoclasts (arrows) is less abundant in the OVX group than in the Sham and ZOL groups (a). The osteoclasts are distinctive by their multiple nuclei and very large cellular sizes, which were confirmed by staining for TRAP (b), a marker for osteoclasts. The number of TUNEL-positive osteoclasts and the staining intensity of individual osteoclasts are both more in the OVX group than the sham and ZOL groups at both time points (a), which is also confirmed by the quantitation of the average TUNEL staining intensity of five randomly selected areas per animal (c). (Data are presented as mean \pm SD. ** indicate a $P < 0.01$, respectively, when compared with the Sham group; # and ## indicate a $P < 0.05$ and 0.01 , respectively, when compared with the OVX group.) (A color version of this figure is available in the online journal.)

Table 1. The seral levels of CTX-I and PINP.

Groups	Sham	OVX	ZOL-20	F	P
The results of serums in 4 weeks					
CTX-I (ng/mL)	1.78 \pm 0.171	5.34 \pm 0.551***	1.99 \pm 0.242###	91.740	<0.001
PINP (pg/mL)	398.30 \pm 41.291	721.24 \pm 47.086*	492.31 \pm 21.279	56.760	<0.001
The results of serums in 12 weeks					
CTX-I (ng/mL)	2.67 \pm 0.284	3.83 \pm 0.218*	2.04 \pm 0.311##	33.000	<0.001
PINP (pg/mL)	739.90 \pm 100.505	917.43 \pm 27.086	592.03 \pm 56.814#	16.990	0.003

ZOL: zoledronic acid; OVX: ovariectomy; CTX-I: C-terminal telopeptide of type I collagen, bone resorption marker; PINP: N-terminal propeptide of type I procollagen, bone formation marker.

Note: Data are presented as mean \pm SD. *Significantly different when comparing the sham group with the OVX or ZOL group. #Values differ significantly from OVX (OVX vs. ZOL-20. At 4 weeks, CTX-I: Sham vs. OVX (** $P < 0.001$), OVX vs. ZOL-20 (### $P < 0.001$), and PINP: OVX vs. Sham or ZOL-20 (* $P < 0.05$). At 12 weeks, CTX-I, Sham vs. OVX (* $P < 0.05$), OVX vs. ZOL-20 (## $P < 0.01$), and PINP, OVX vs. ZOL-20 (# $P < 0.05$).

between the sham and OVX groups, while the number of apoptotic osteoclasts in this group was almost identical to that in the sham group. At the later time point, the number of apoptotic osteoblasts and osteoclasts in the Sham and ZOL groups was similar but still differed significantly from their counterpart in the OVX group. These data collectively suggest that ZOL not only inhibits OVX-caused apoptosis of osteoblasts but also, more significantly, counteracts OVX-caused inhibition of apoptosis of osteoclasts or even directly enhances apoptosis of osteoclasts, at least during the earlier time period.

Serum levels of bone turnover markers CTX-I and PINP

The International Osteoporosis Foundation and the International Federation of Clinical Chemistry (IFCC) Bone Marker Standards Working Group have recommended the serum levels of the N-terminal propeptide of type I procollagen (PINP) and C-terminal telopeptide of

type I collagen (CTX-I) as the reference markers for bone turnover that reflect changes in bone metabolism induced by anti-osteoporotic treatment.³⁷ Anti-resorptive drugs induce rapid dose-dependent decreases in bone resorption, whereas bone formation stimulating medications increase the levels of these bone formation markers.^{37,38} Compared with the sham group at the fourth-week time point, the serum CTX-I and PINP levels in the OVX group were increased, suggesting that OVX enhances the transformation of bone tissues. However, these two bone transformation markers were decreased in the ZOL group to the levels seen in the sham group (Table 1).

Effect of OVX and ZOL on RANKL and some NF- κ B components in the mandible

Positive IHC staining for RANKL was observed mainly in osteoclasts due to their multiple nuclei and very large cellular size, whereas the staining in other cell types that are

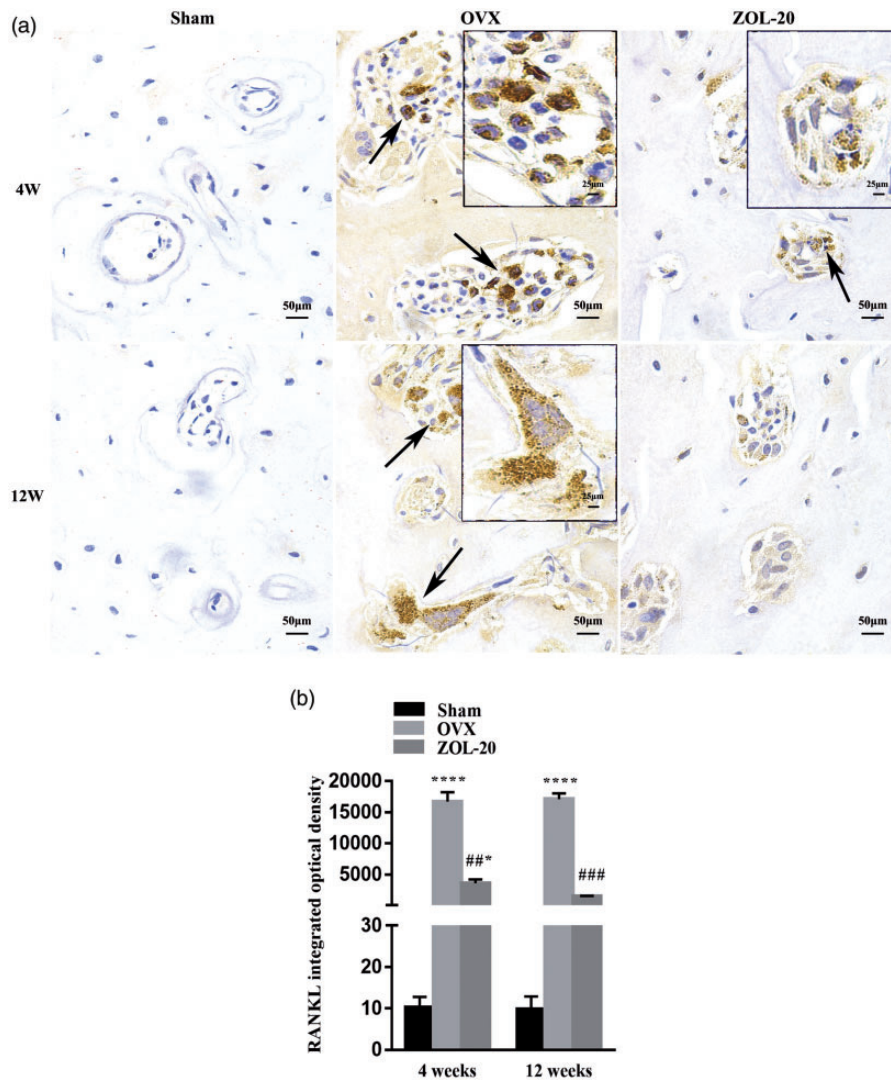


Figure 7. IHC staining for RANKL in the mandible. RANKL positive cells are mainly osteoclasts (a). The number of positive osteoclasts and the average staining intensity of individual osteoclasts are both higher in the OVX group than in the sham and ZOL groups at both time points (a); quantitation of average staining intensity, which is mainly contributed by osteoclasts, of five randomly selected areas per animal shows similar results (b). (Data are presented as mean \pm SD. * and **** indicate a $P < 0.05$ and 0.0001 , respectively, when compared with the sham group; ## and ### indicate a $P < 0.01$ and 0.001 , respectively, when compared with the OVX group.) (A color version of this figure is available in the online journal.)

much smaller was challenging to quantify (Figure 7(a)). Similarly, positive IHC staining for the p65 component of the NF- κ B complex was also much more clear in the osteoclasts than in other cell types (Figure 8(a)). For both RANKL and p65, the number of positive osteoclasts as well as the staining intensity in individual osteoclasts were both much higher in the sham and ZOL groups than in the OVX group at both time points (Figures 7(a) and 8(a)). Quantification of average staining intensity of randomly selected areas, which was mainly contributed by the large osteoclasts, also resulted in the same data (Figures 7(b) and 8(b)). These data suggest that OVX induces the protein expression of these two genes mainly in osteoclasts, while ZOL counteracts the induction.

WB assay showed that at both time points OVX upregulated the RANKL protein level in the mandible tissue compared with the sham operation, whereas ZOL attenuated the induction. This was shown by quantification and statistical comparison of the density of the WB bands based on

the ratio of the density of RANKL to that of the corresponding β -actin included as the protein loading control (Figure 9). WB also showed similar changes in the total p65 level as well as its phosphorylated form at both time points (Figure 9). The total protein of I κ B- α , which is an inhibitory component of the NF- κ B complex, did not show obvious differences among the three groups. However, its phosphorylated form, which is known to result in quick degradation of I κ B- α via a ubiquitin pathway, was significantly increased by OVX, especially at the fourth-week time point; this induction was attenuated by ZOL (Figure 9).

Discussion

It has been shown that in OVX rats, the trabecular bone of the femoral neck and mandible becomes thinner, while the morphology of the bone cortex shows limited change, including the cortex of the femur and mandible.³⁹

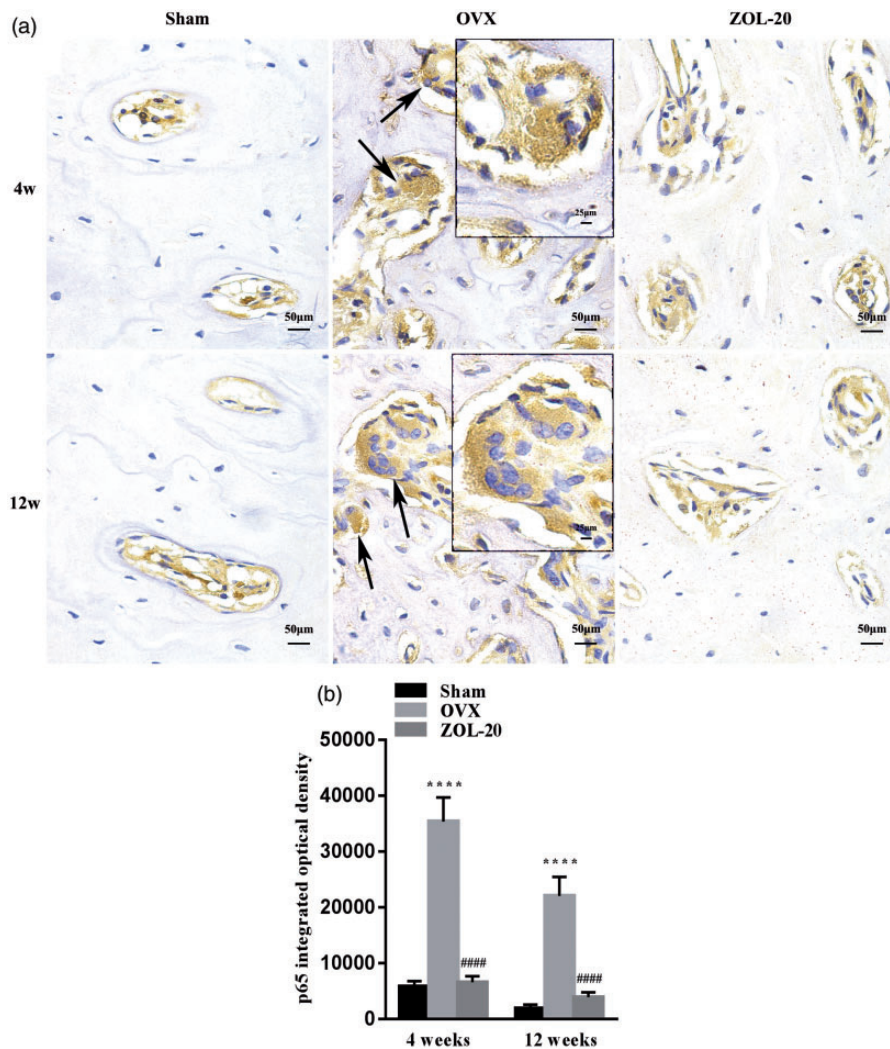


Figure 8. IHC staining for the p65 component of the NF- κ B complex in the mandible. Positive cells are mainly osteoclasts (a). The number of positive osteoclasts and the average staining intensity of individual osteoclasts are both higher in the OVX group than in the Sham and ZOL groups at both time points (a); quantification of average staining intensity, which is mainly contributed by osteoclasts, of five randomly selected areas per animal shows similar results (b). (Data are presented as mean \pm SD. **** indicate a $P < 0.0001$, respectively, when compared with the Sham group; ##### indicate a $P < 0.0001$, respectively, when compared with the OVX group.). (A color version of this figure is available in the online journal.)

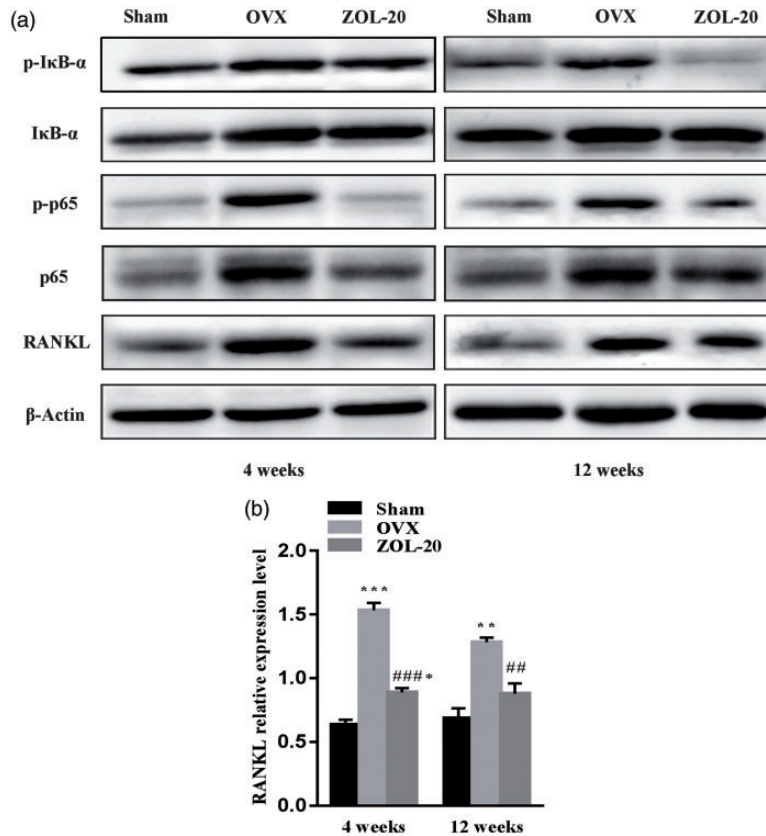


Figure 9. WB assay of RANKL and certain NF- κ B components in the mandibular tissue. (a) OVX induces RANKL as well as the total protein and the phosphorylated form of not only p65 but also I κ B- α four weeks post OVX, while ZOL prevents these effects of OVX. These changes are still discerned but much less evident at the later time point. (b) Quantitation of the band intensity shows that these differences, after correction with the signal of β -Actin included for the protein loading control, are still statistically significant. Data are presented as mean \pm SD. *, ** and *** indicate a $P < 0.05$, 0.01 and 0.001, respectively, when compared with the Sham group; ## and ### indicate a $P < 0.01$ and 0.001, respectively, when compared with the OVX group.

However, this topographic discrepancy has been considered to be temporary after OVX.⁴⁰ To avoid this potential problem of temporality, we studied the effect of a single low dose of ZOL in an OVX model at 4 and 12 weeks post ovary removal. We observed that ZOL at only 20 μ g/kg could counteract the OVX-caused bone loss in the alveolar fossa of the mandible, which was already evident at the fourth-week time point. The mandibular morphology showed that the ZOL treatment increased the cancellous bone density and the trabecular structure connections in the OVX rats to the levels seen in the sham-operated animals. These observations are in line with the report from Porras *et al.* that ZOL can reverse the osteoporosis-caused bone resorption and bone damage⁴¹ and dovetail with the observations of Soares *et al.* that ZOL can promote the corticalization and trabecular thickening of the mandibular alveolar bone in rats.⁴² The effects of ZOL seem to be long lasting, since the effects are still evident 12 weeks post ZOL administration. This indirectly supports the opinion that bisphosphonates have a very strong adhesion to bone, with a half-life of several years,⁴³ and thus its administration can be discontinued after several years of treatments while still maintaining the anti-fracture effects.⁴⁴

At the cellular level, the mechanism behind the effects of ZOL includes enhancing apoptosis of osteoclasts, thus decreasing their number, and inhibiting apoptosis of

osteoblasts, thus increasing their number; both of which collectively result in increased bone growth. Other researchers also consider that bisphosphonates can enhance the replication of osteoblasts and sustain their survival.^{24,45} High bone turnover level, which can be reflected by the high levels of CTX-1 and PINP according to the IFCC,⁴⁶ is a typical feature of postmenopausal women.⁴⁶ We show herein that OVX rats manifest similar increases in the serum levels of CTX-1 and PINP, indicating that the post OVX life in the rat nicely resembles the postmenopausal environment. We have also observed that ZOL attenuates the OVX-caused increase in the CTX-1 and PINP levels, which dovetails with the reports that ZOL can reduce the levels of PINP and CTX-I,⁴⁷ thus further suggesting that the anti-decomposition effect of ZOL may lead to the decrease in bone turnover rate.⁴⁸ Therefore, our observations suggest that the IFCC recommendation of using CTX-1 and PINP levels for bone safety of ZOL application⁴⁹ may be used for stomatology as well.

At the molecular level, OVX induces RANKL, the total protein level of p65, and the phosphorylation of p65 and I κ B- α mainly in the osteoclasts of the mandible, which presumably enhance differentiation of osteoclasts and in turn the loss of bone mass.⁵⁰⁻⁵² The counteraction of ZOL on OVX-caused bone mass loss may be mechanistically attributed, in part, to its inhibition of the OVX-caused activation

of the RANKL-NF- κ B signalling pathway that leads to enhanced differentiation of osteoclasts.^{24,28,34} It cannot be excluded that the increase in the number of apoptotic osteoblasts in the OVX group and the decrease in the number of apoptotic osteoblasts in the ZOL group also involve the same molecular mechanism. However, this hypothetical thinking remains to be further determined, as osteoblasts are much smaller in size and it is difficult to quantify their IHC staining intensity.

In summation, in this study we observed that OVX caused bone mass loss in the mandible, especially at an earlier period post OVX. These effects involved an increase in apoptotic osteoblasts and decrease in apoptotic osteoclasts at the cellular level. At the molecular level, activation of RANKL-NF- κ B signalling in the osteoclasts may occur to enhance their differentiation, leading to the enhancement of bone resorption. Treatment with a single low dose of ZOL can counteract the OVX-caused loss of bone mass, which may be elicited via counteracting the abovementioned cellular and molecular effects of OVX.

AUTHORS' CONTRIBUTIONS

JL conceived and designed the research. YTC, QZ, HH performed the experiments. YTC, JL performed preliminary data analysis. ZLT and HM supervised the investigation and proof checked data for error. The article was written and revised by: YTC, JL, LZ, WH. DJL reevaluated the pathology and revised the manuscript. All authors have read and approved the final manuscript.



DECLARATION OF CONFLICTING INTERESTS

The author(s) declared no potential conflicts of interest with respect to the research, authorship, and/or publication of this article.

FUNDING

The author(s) disclosed receipt of the following financial support for the research, authorship, and/or publication of this article: This work was supported by the Natural Science Foundation of China (Grant Nos. 82060207) and by the Science and Technology Foundation of Guizhou Province (Grant No. (2016)1124).

ORCID iDs

Yu-Ting Cheng  <https://orcid.org/0000-0002-0300-9460>
Jian Liao  <https://orcid.org/0000-0003-3519-4485>

REFERENCES

- Buser D, Sennerby L, De Bruyn H. Modern implant dentistry based on osseointegration: 50 years of progress, current trends and open questions. *Periodontol* 2000 2017;**73**:7–21
- Charatchaiwanna A, Rojsiraphisa T, Aunmeungtong W, Reichart PA, Khongkhunthian P. Mathematical equations for dental implant stability patterns during the osseointegration period, based on previous resonance frequency analysis studies. *Clin Implant Dent Relat Res* 2019;**21**:1028–40
- Liu Y, Li Z, Arioka M, Wang L, Bao C, Helms JA. WNT3A accelerates delayed alveolar bone repair in ovariectomized mice. *Osteoporos Int* 2019;**30**:1873–85
- Liu X, Zhang R, Zhou Y, Yang Y, Si H, Li X, Liu L. The effect of astragalus extractive on alveolar bone rebuilding progress of tooth extracted socket of ovariectomized rats. *Afr J Tradit Complement Altern Med* 2014;**11**:91–8
- de Medeiros F, Kudo G, Leme BG, Saraiva PP, Verri FR, Honorio HM, Pellizzer EP, Santiago JJ. Dental implants in patients with osteoporosis: a systematic review with meta-analysis. *Int J Oral Maxillofac Surg* 2018;**47**:480–91
- Chai J, Chau AC, Chu FC, Chow TW. Diagnostic performance of mandibular bone density measurements in assessing osteoporotic status. *Int J Oral Maxillofac Implants* 2014;**29**:667–74
- Harvey N, Dennison E, Cooper C. Osteoporosis: impact on health and economics. *Nat Rev Rheumatol* 2010;**6**:99–105
- Oden A, McCloskey EV, Kanis JA, Harvey NC, Johansson H. Burden of high fracture probability worldwide: secular increases 2010–2040. *Osteoporos Int* 2015;**26**:2243–8
- Thulker J, Singh S, Sharma S, Thulker T. Preventable risk factors for osteoporosis in postmenopausal women: systematic review and meta-analysis. *J Midlife Health* 2016;**7**:108–13
- Xu SW, Yu R, Zhao GF, Wang JW. Early period of fracture healing in ovariectomized rats. *Chin J Traumatol* 2003;**6**:160–6
- Kubo T, Shiga T, Hashimoto J, Yoshioka M, Honjo H, Urabe M, Kitajima I, Semba I, Hirasawa Y. Osteoporosis influences the late period of fracture healing in a rat model prepared by ovariectomy and low calcium diet. *J Steroid Biochem Mol Biol* 1999;**68**:197–202
- Teitelbaum SL. Bone resorption by osteoclasts. *Science* 2000;**289**:1504–8
- Luo J, Yang Z, Ma Y, Yue Z, Lin H, Qu G, Huang J, Dai W, Li C, Zheng C, Xu L, Chen H, Wang J, Li D, Siwko S, Penninger JM, Ning G, Xiao J, Liu M. LGR4 is a receptor for RANKL and negatively regulates osteoclast differentiation and bone resorption. *Nat Med* 2016;**22**:539–46
- Tan EM, Li L, Indran IR, Chew N, Yong EL. TRAF6 mediates suppression of osteoclastogenesis and prevention of ovariectomy-induced bone loss by a novel prenylflavonoid. *J Bone Miner Res* 2017;**32**:846–60
- Lu J, Liu F, Liu D, Du H, Hao J, Yang X, Cui W. Amlodipine and atorvastatin improved hypertensive cardiac hypertrophy through regulation of receptor activator of nuclear factor kappa B ligand/receptor activator of nuclear factor kappa B/osteoprotegerin system in spontaneous hypertension rats. *Exp Biol Med* 2016;**241**:1237–49
- Compston JE, McClung MR, Leslie WD. Osteoporosis. *Lancet* 2019;**393**:364–76
- O'Carrigan B, Wong MH, Willson ML, Stockler MR, Pavlakis N, Goodwin A. Bisphosphonates and other bone agents for breast cancer. *Cochrane Database Syst Rev* 2017;**10**:D3474
- Chandran T, Venkatachalam I. Efficacy and safety of denosumab compared to bisphosphonates in improving bone strength in postmenopausal osteoporosis: a systematic review. *Singapore Med J* 2019;**60**:364–78
- Grey A, Bolland MJ, Horne A, Mihov B, Gamble G, Reid IR. Duration of antiresorptive activity of zoledronate in postmenopausal women with osteopenia: a randomized, controlled multidose trial. *CMAJ* 2017;**189**:E1130–6
- Messer JG, Mendieta CJ, Jiron JM, Castillo EJ, Van Poznak C, Bhattacharyya N, Kimmel DB, Aguirre JI. Zoledronic acid increases the prevalence of medication-related osteonecrosis of the jaw in a dose dependent manner in rice rats (*oryzomys palustris*) with localized periodontitis. *Bone* 2018;**108**:79–88
- Dhillon S. Zoledronic acid (reclast®, aclasta®): a review in osteoporosis. *Drugs* 2016;**76**:1683–97
- Qi M, Hu J, Li J, Li J, Dong W, Feng X, Yu J. Effect of zoledronate acid treatment on osseointegration and fixation of implants in autologous iliac bone grafts in ovariectomized rabbits. *Bone* 2012;**50**:119–27
- Mardas N, Busetti J, de Figueiredo JA, Mezzomo LA, Scarparo RK, Donos N. Guided bone regeneration in osteoporotic conditions following treatment with zoledronic acid. *Clin Oral Implants Res* 2017;**28**:362–71
- Li M, Wan P, Wang W, Yang K, Zhang Y, Han Y. Regulation of osteogenesis and osteoclastogenesis by zoledronic acid loaded on biodegradable magnesium-strontium alloy. *Sci Rep* 2019;**9**:933

25. Benford HL, McGowan NW, Helfrich MH, Nuttall ME, Rogers MJ. Visualization of bisphosphonate-induced caspase-3 activity in apoptotic osteoclasts in vitro. *Bone* 2001;**28**:465–73
26. Tai TW, Chen CY, Su FC, Tu YK, Tsai TT, Lin CF, Jou IM. Reactive oxygen species are required for zoledronic acid-induced apoptosis in osteoclast precursors and mature osteoclast-like cells. *Sci Rep* 2017;**7**:44245
27. Tai TW, Su FC, Chen CY, Jou IM, Lin CF. Activation of p38 MAPK-regulated Bcl-xL signaling increases survival against zoledronic acid-induced apoptosis in osteoclast precursors. *Bone* 2014;**67**:166–74
28. Kimachi K, Kajiya H, Nakayama S, Ikebe T, Okabe K. Zoledronic acid inhibits RANK expression and migration of osteoclast precursors during osteoclastogenesis. *Naunyn Schmiedebergs Arch Pharmacol* 2011;**383**:297–308
29. Furuya M, Kikuta J, Fujimori S, Seno S, Maeda H, Shirazaki M, Uenaka M, Mizuno H, Iwamoto Y, Morimoto A, Hashimoto K, Ito T, Isogai Y, Kashii M, Kaito T, Ohba S, Chung UI, Lichtler AC, Kikuchi K, Matsuda H, Yoshikawa H, Ishii M. Direct cell-cell contact between mature osteoblasts and osteoclasts dynamically controls their functions in vivo. *Nat Commun* 2018;**9**:300
30. Greiner S, Kadow-Romacker A, Schmidmaier G, Wildemann B. Cocultures of osteoblasts and osteoclasts are influenced by local application of zoledronic acid incorporated in a poly(D,L-lactide) implant coating. *J Biomed Mater Res A* 2009;**91**:288–95
31. Ayan M, Dolanmaz D, Mihmanli A, Ayan A, Kurkcu M. The effect of systemically administrated zoledronic acid on the osseointegration of dental implants. *Oral Dis* 2012;**18**:802–8
32. Dikicier S, Dikicier E, Karacayli U, Erguder B. Radiodensitometric study for evaluation of bone mineral density around dental implants after zoledronic acid treatment in ovariectomized rats. *Med Oral Patol Oral* 2017;**22**:e377–82
33. von Knoch M, Wedemeyer C, Pingsmann A, von Knoch F, Hilken G, Sprecher C, Henschke F, Barden B, Loer F. The decrease of particle-induced osteolysis after a single dose of bisphosphonate. *Biomaterials* 2005;**26**:1803–8
34. Huang XL, Huang LY, Cheng YT, Li F, Zhou Q, Wu C, Shi QH, Guan ZZ, Liao J, Hong W. Zoledronic acid inhibits osteoclast differentiation and function through the regulation of NF-kappaB and JNK signalling pathways. *Int J Mol Med* 2019;**44**:582–92
35. Kharode YP, Sharp MC, Bodine PV. Utility of the ovariectomized rat as a model for human osteoporosis in drug discovery. *Methods Mol Biol* 2008;**455**:111–24
36. Contie S, Voorzanger-Rousselot N, Litvin J, Bonnet N, Ferrari S, Clezardin P, Garnero P. Development of a new ELISA for serum periostin: evaluation of growth-related changes and bisphosphonate treatment in mice. *Calcif Tissue Int* 2010;**87**:341–50
37. Szulc P, Naylor K, Hoyle NR, Eastell R, Leary ET. Use of CTX-I and PINP as bone turnover markers: national bone health alliance recommendations to standardize sample handling and patient preparation to reduce pre-analytical variability. *Osteoporos Int* 2017;**28**:2541–56
38. Szulc P. Bone turnover: biology and assessment tools. *Best Pract Res Clin Endocrinol Metab* 2018;**32**:725–38
39. Hsu PY, Tsai MT, Wang SP, Chen YJ, Wu J, Hsu JT. Cortical bone morphological and trabecular bone microarchitectural changes in the mandible and femoral neck of ovariectomized rats. *PLoS One* 2016;**11**:e154367
40. Johnston BD, Ward WE. The ovariectomized rat as a model for studying alveolar bone loss in postmenopausal women. *Biomed Res Int* 2015;**2015**:635023
41. Surmelioglu O, Aydogan FK, Ozdemir S, Tarkan O, Uguz A, Tuncer U, Aydogan LB. The effect of zoledronic acid on middle ear osteoporosis: an animal study. *Ear Nose Throat J* 2018;**97**:E44–8
42. Soares M, Van Dessel J, Jacobs R, Da SSP, Cestari TM, Garlet GP, Duarte M, Imada T, Lambrechts I, Rubira-Bullen I. Zoledronic acid induces site-specific structural changes and decreases vascular area in the alveolar bone. *J Oral Maxillofac Surg* 2018;**76**:1893–901
43. Porras AG, Holland SD, Gertz BJ. Pharmacokinetics of alendronate. *Clin Pharmacokinet* 1999;**36**:315–28
44. Schwartz AV, Bauer DC, Cummings SR, Cauley JA, Ensrud KE, Palermo L, Wallace RB, Hochberg MC, Feldstein AC, Lombardi A, Black DM. Efficacy of continued alendronate for fractures in women with and without prevalent vertebral fracture: the FLEX trial. *J Bone Miner Res* 2010;**25**:976–82
45. Maruotti N, Corrado A, Neve A, Cantatore FP. Bisphosphonates: effects on osteoblast. *Eur J Clin Pharmacol* 2012;**68**:1013–8
46. Cavalier E, Bergmann P, Bruyere O, Delanaye P, Durnez A, Devogelaer JP, Ferrari SL, Gielen E, Goemaere S, Kaufman JM, Toukap AN, Reginster JY, Rousseau AF, Rozenberg S, Scheen AJ, Body JJ. The role of biochemical of bone turnover markers in osteoporosis and metabolic bone disease: a consensus paper of the Belgian bone club. *Osteoporos Int* 2016;**27**:2181–95
47. Koldkjaer SA, Harslof T, Langdahl B. Treatment with zoledronic acid subsequent to odanacatib prevents bone loss in postmenopausal women with osteoporosis. *Osteoporos Int* 2019;**30**:995–1002
48. Hao Y, Wang X, Wang L, Lu Y, Mao Z, Ge S, Dai K. Zoledronic acid suppresses callus remodeling but enhances callus strength in an osteoporotic rat model of fracture healing. *Bone* 2015;**81**:702–11
49. Eastell R, Szulc P. Use of bone turnover markers in postmenopausal osteoporosis. *Lancet Diabetes Endocrinol* 2017;**5**:908–23
50. Chen K, Yan Z, Wang Y, Yang Y, Cai M, Huang C, Li B, Yang M, Zhou X, Wei X, Yang C, Chen Z, Zhai X, Li M. Shikonin mitigates ovariectomy-induced bone loss and RANKL-induced osteoclastogenesis via TRAF6-mediated signaling pathways. *Biomed Pharmacother* 2020;**126**:110067
51. Chang AR, Cho TH, Hwang SJ. Receptor activator of nuclear factor Kappa-B ligand-induced local osteoporotic canine mandible model for the evaluation of peri-implant bone regeneration. *Tissue Eng Part C Methods* 2017;**23**:781–94
52. Park JH, Lee Nk, Lee S. Current understanding of RANK signaling in osteoclast differentiation and maturation. *Mol Cells* 2017;**40**:706–13

(Received October 3, 2020, Accepted March 24, 2021)